BEAM DYNAMICS STUDY OF THE INTERMEDIATE ENERGY X-RAY WIGGLER FOR THE ADVANCED PHOTON SOURCE*

A. Xiao†, M. Borland, L. Emery, M. Jaski, V. Sajaev
ANL, Argonne, IL 60439, USA

Abstract

An intermediate-energy x-ray (IEX) helical wiggler is planned for the APS storage ring. Because of its high field and rapid field roll-off, the disturbance to the beam dynamics is large and needs to be well understood before the installation. We present a new method of fitting the magnetic field to an analytical wiggler model, which simplifies the usual nonlinear fitting problem and guarantees the best fit. The fitting method was validated by comparison to an analytical method.

INTRODUCTION

To meet user requirements, an intermediate-energy x-ray (IEX) helical wiggler is planned for the APS storage ring. To reduce the chance of a unpleasant surprise, a detailed beam dynamics study was carried out, and the magnet design was modified accordingly.

Insertion devices (IDs) often perturb the beam. The linear perturbation is often corrected locally by adding small multipole correctors to the ends of the ID or using existing accelerator steering and focusing knobs. The overall machine performance is usually kept unchanged without great difficulty. Since nonlinear perturbations are more difficult to correct, they should be kept within tolerable levels through careful magnet design and modeling. Assuming a sinusoidal model of the magnetic field, the nonlinear kick in the x-plane for a horizontally deflecting wiggler (the simplest case is selected for illustration) is given by

$$\Delta x'(x) = -\frac{L_w}{(E/e)^2}\left(\frac{\lambda_w}{2\pi}\right)^2 B_{y0}^2 \frac{d}{dx}F^2(x), \qquad (1)$$

where L_w is the length of the wiggler, E is the beam energy, λ_w is the period length, B_{y0}^2 is the peak field, and $F(x) = B_y(x)/B_y(0)$. The nonlinearity comes from the roll-off in $F(x)$.

Compared with a planar wiggler, helical wigglers normally have narrow poles because they need to have the vertical and horizontal poles interleaved to provide alternating B_y and B_x fields. The narrowing results in a larger $\frac{d}{dx}F^2(x)$ term close to the axis (beam center). In addition, the APS device has a long period length to generate the required low-energy synchrotron radiation. Both factors contribute to larger than usual nonlinear effects.

* Work supported by the U. S. Department of Energy, Office of Science, Office of Basic Energy Sciences, under Contract No. DE-AC02-06CH11357.

† xiaoam@aps.anl.gov

To evaluate the beam dynamics implications, we started by fitting the numerical 3D field data to the analytical field-expansion functions (harmonics) used by the `CWIGGLER` element in `elegant [1]`. This element uses the canonical tracking method by [2], but is necessarily very slow. The calculation of dynamic aperture (DA) and local momentum aperture (LMA) is a process involving particle tracking for hundreds of turns, which is computationally expensive if `CWIGGLER` is used. To shorten the tracking time, we replace the wiggler element with a kick map element `UKICKMAP` ($(\Delta x', \Delta y') = \vec{f}(x_0, y_0)$), which is calculated once by tracking uniformly distributed grid particles in $x-y$ plane with $(x', y')_0 = 0$ through the `CWIGGLER` element (the "long way").

In this paper, we demonstrate in detail how the methods described above are applied to the IEX magnet design and show the simulation results. The kick map can also be calculated directly from the field map using Elleaume's method [3]. We present a comparison of results for these two methods.

FITTING METHOD

The IEX device can be operated in three ways and provide a pure horizontal (H-mode), pure vertical (V-mode), and elliptically (C-mode) polarized x-ray beam to experiment users. Its magnetic field can be expressed as:

$$\begin{aligned} B_x^H &= B_0^H \textstyle\sum_{m,n} A_{mn}^H \frac{k_{x,mn}^H}{k_{y,mn}^H} \sin(k_{x,mn}^H x) \\ &\quad \cdot \sinh(k_{y,mn}^H y) \cdot \cos(k_{zn} z) \\ B_y^H &= -B_0^H \textstyle\sum_{m,n} A_{mn}^H \cos(k_{x,mn}^H x) \\ &\quad \cdot \cosh(k_{y,mn}^H y) \cdot \cos(k_{zn} z), \end{aligned} \qquad (2)$$

with $(k_{y,mn}^H)^2 = (k_{x,mn}^H)^2 + (k_{zn})^2$ for the field generated from the two middle poles, and

$$\begin{aligned} B_x^V &= B_0^V \textstyle\sum_{m,n} A_{mn}^V \cos(k_{x,mn}^V x) \\ &\quad \cdot \cosh(k_{y,mn}^V y) \cdot \cos(k_{zn} z + \tfrac{\pi}{2}) \\ B_y^V &= B_0^V \textstyle\sum_{m,n} A_{mn}^V \frac{k_{y,mn}^V}{k_{x,mn}^V} \sin(k_{x,mn}^V x) \\ &\quad \cdot \sinh(k_{y,mn}^V y) \cdot \cos(k_{zn} z + \tfrac{\pi}{2}), \end{aligned} \qquad (3)$$

with $(k_{y,mn}^V)^2 = (k_{x,mn}^V)^2 + (k_{zn})^2$ for the field generated from the four side poles. Here, $k_{zn} = 2\pi n/\lambda_u$, λ_u is the

period, B_0^H and B_0^V are the maximum on-axis horizontal and vertical fields, respectively. The total field is given by

$$B_y^C = B_y^H + B_y^V$$
$$B_x^C = B_x^H + B_x^V. \quad (4)$$

The calculated field data is provided on a 3D (x, y, z) grid. There are many ways to fit it to the analytical model expressed in Eqs. 2 through 4. Using the H-mode field (Eq. 2) as an example, we introduce a simplified method that allows us to obtain the optimum fit. First, we perform harmonic analysis (FFT) of B_y (we drop the superscript H from here) vs z at each (x, y) grid line. The resulting amplitude $F_n(x, y)$ for each harmonic n is

$$F_n(x, y) = -B_0 \sum_m A_{mn} \cos(k_{x,mn} x) \cdot \cosh(k_{y,mn} y), \quad (5)$$

where A_{mn} and $k_{x,mn}$ are unknown variables, and $k_{y,mn}$ are variables related to $k_{x,mn}$ and k_{zn}. Since there is no periodic boundary condition in the transverse plane, the $k_{x,mn}$ do not necessarily form a harmonic series. However, to simplify the problem, we use the harmonic decomposition $k_{x,mn} = m \cdot k_{x,1n}$ in the transverse plane also. In such a case we still have A_{mn} and $k_{x,1n}$ as unknowns. For a field with a transverse profile B_y at $y = 0$ that differs from a cosine shape, a number of A_{mn} coefficients are needed to get a good fit. The fitting of nonlinear equations with many free parameters is always troublesome, and there is no guarantee for the best result. By examining Eq. 5, we see that if $k_{x,1n}$ is known (so determing $k_{x,mn} = m \cdot k_{x,1n}$), the equation simplifies to a linear equation in A_{mn}. The fit for $F_n(x, y)$ at all (x, y) grid points together forms a set of linear equations, which can be solved using the singular value decomposition (SVD) method. The resulting A_{mn} are the best fit for that particular $k_{x,1n}$ when the number of equations is larger than n. By scanning $k_{x,1n}$ in a reasonable range, the overall best fit is obtained. Figure 1 shows an example result of this scan-fit combination for $n = 1$. Figure 2 shows the fitting result for the IEX magnet working at C-mode.

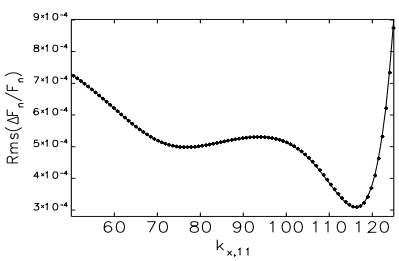

Figure 1: Example: residual fitting error Rms$(\Delta F_n/F_n)$ vs. $k_{x,11}$ $(n = 1)$.

SIMULATION OF IEX

Once the fit is obtained, the remaining steps are are straightforward. First, using the fit as the input of the

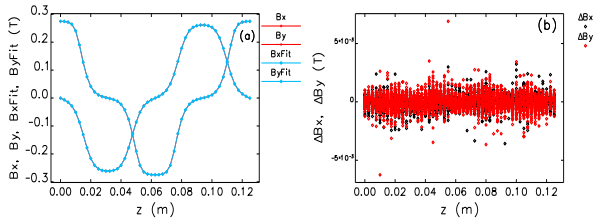

Figure 2: IEX fitting result (C-mode): (a) on-axis field; (b) overall fitting error for a region of ±17 mm (x) × ±3 mm (y).

CWIGGLER element, a grid of particles with zero longitudinal emittance, $(x', y')_0 = 0$, and a transverse distribution covering the entire vacuum chamber interior region are tracked using the accurate symplectic integration method. A kick map $(\Delta x', \Delta y') = \vec{f}(x_0, y_0)$ is built from the tracking results. Figure 3 shows the kick maps in C-mode for two IEX designs. In addition, we show results for a hypothetical double-length circular polarized undulator (CPU), a device that is now in daily operation, but that in reality has half the length of the 4.8-m IEX device.

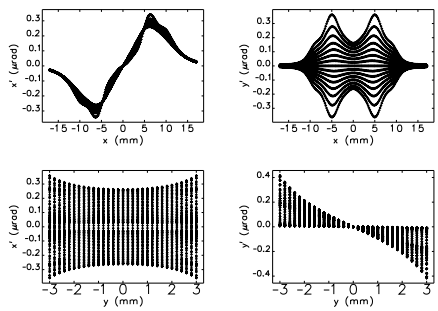

Figure 3: Kick map of IEX (1 period, C-mode).

The DA and LMA are calculated using the resulting kick map. To examine the IEX effect, the simulation results are compared to those without any IDs and those with a double-length CPU. For the original IEX design (IEX1), results show that there is no obvious LMA change but the DA decreased significantly. Based on these findings, a new IEX design (IEX2) was made with extra effort on reducing the roll-off factor ($\frac{d}{dx}F^2(x)$ in Eq. 1). Calculated kick maps of IEX1, IEX2, and CPU are shown in Figure 4. The

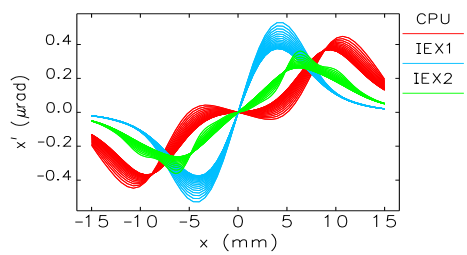

Figure 4: Kick map - 1 period, C-mode.

corresponding DA and MA results are shown in Figure 5. From the simulation results, we see that for the new IEX design (IEX2), the DA is the same as APS. The installation of IEX should pose no significant beam dynamics issue in APS operation.

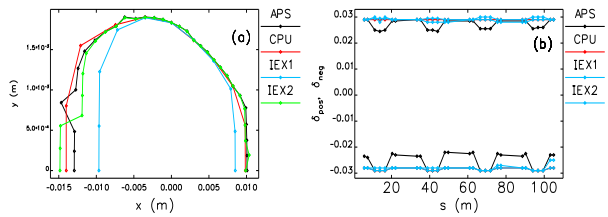

Figure 5: Simulation results: (a) DA; (b) MA. (APS: lattice without IDs; CPU: APS+CPU; IEX1: APS+IEX, and IEX2: APS+IEX2).

ELLEAUME'S METHOD

Elleaume reported an analytical method [3] to calculate the undulator kick map in 1992, which is widely used. To be confident that the use of the fitting model is valid, we also applied Elleaume's method to the same IEX data. To demonstrate our work, we re-write Elleaume's Formula (Eq. (5) in [3]) here. If the magnetic field satisfies conditions:

$$\int_{-\infty}^{\infty} B_x ds = 0 \qquad \int_{-\infty}^{\infty}\int_{-\infty}^{s} B_x ds' ds = 0$$
$$\int_{-\infty}^{\infty} B_y ds = 0 \qquad \int_{-\infty}^{\infty}\int_{-\infty}^{s} B_y ds' ds = 0, \quad (6)$$

for a particle with initial angle equal to zero $\frac{dx}{ds}(-\infty) = \frac{dy}{ds}(-\infty) = 0$, its angle after crossing the magnetic field region can be written as Eq. 7:

$$\frac{dx}{ds}(\infty) = -\frac{\alpha^2}{2}\int_{-\infty}^{\infty}\frac{\partial}{\partial x}\Phi(x,y,s)ds + o(\alpha^3)$$
$$\frac{dy}{ds}(\infty) = -\frac{\alpha^2}{2}\int_{-\infty}^{\infty}\frac{\partial}{\partial y}\Phi(x,y,s)ds + o(\alpha^3) \quad (7)$$
$$\Phi(x,y,s) = \left(\int_{-\infty}^{s} B_x ds\right)^2 + \left(\int_{-\infty}^{s} B_y ds\right)^2,$$

where $\alpha = e/\gamma m_0 c$, e is the electron charge, m_0 is the mass, and c is the speed of light.

Results of applying Eq. 7 to the IEX H-mode are shown in Figure 6. Since the kick map from Elleaume's method is calculated using the discrete data points, the resulting kick map is coarse compared with the fitting method. However, they are very similar. The relative calculation error is shown in Figure 7. Application to the V-mode gave similar results. Direct application to one period field of the C-mode is invalid because the double integration condition in Eq. 6 can not be satisfied in both planes at the same time. The formula is only valid for the full length of the device for the C-mode.

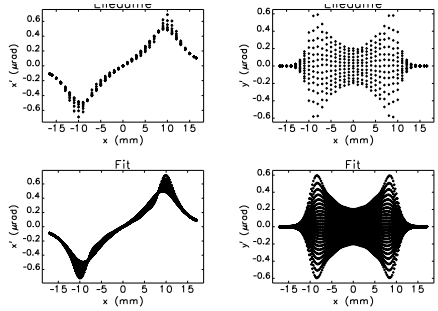

Figure 6: Kick map of IEX H-mode: Top - calculated from the Elleaume method; Bottom - calculated from the fitted model.

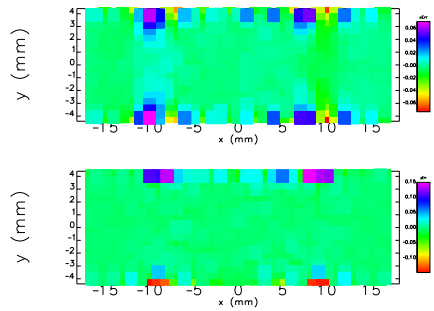

Figure 7: Relative error of calculated kick map (IEX H-mode) ($err = (kick_{Elleaume} - kick_{Fit})/Max(kick_{Fit})$).

SUMMARY

A simplified fitting method was developed that simplifies the fitting of multivariate nonlinear equations to a one-dimensional parameter scan plus solution of linear equations. This reformulation of the problem guarantees finding the best fit. Simulation results show that the original IEX design has a large magnetic field roll-off close to the beam axis that imposes strong nonlinear kicks on the beams, thus impacting DA noticeably. The revised design reduces this effect and restores the DA, so that no problem is anticipated for APS operation. The kick map of the IEX design was calculated using both the fitting method and the Elleaume method. The results agree with each other quite well, which validates both methods.

REFERENCES

[1] M. Borland, "elegant: A Flexible SDDS-Compliant Code for Accelerator Simulation," Advanced Photon Source, Light Source Note LS-287, September 2000.

[2] Y. K. Wu, E. Forest and D. S. Robin, "Explicit symplectic integrator for s-dependent static magnetic field," Phys. Rev., E68 (2003) 046502.

[3] P. Elleaume, "A New Approach to the Electron Beam Dynamics in Undulators and Wigglers," Proc. of EPAC'92, p.661 (1992); http://www.JACoW.org.